Investigation of electron localization in harmonic emission from asymmetric molecular ion*

Zhang Cai-Ping(张彩萍) and Miao Xiang-Yang(苗向阳)†

College of Physics and Information Engineering, Shanxi Normal University, Linfen 041004, *China*

(Received 11 November 2014; revised manuscript received 1 December 2014; published online 10 February 2015)

We theoretically investigate the electron localization around two nuclei in harmonic emission from asymmetric molecular ion. The results show that the ionization process of electron localized around one nucleus competes with its transfer process to the other nucleus. By increasing the initial vibrational level, more electrons localized around the nucleus D^+ tend to transfer to the nucleus He^{2+} so that the ionizations of electrons localized around the nucleus He^{2+} increase. In this case, the difference in harmonic efficiency between HeH^{2+} and HeD^{2+} decreases while the difference in harmonic spectral structure increases. The evident minimum can be observed in the harmonic spectrum of HeH^{2+} compared with that in the spectral structure of HeD^{2+}, which is due to the strong interference of multiple recombination channels originating from two nuclei. Time-dependent nuclear probability density, electron-nuclear probability density, double-well model, and time-frequency maps are presented to explain the underlying mechanisms.

Keywords: high-order harmonic generation, asymmetric molecular ion, vibrational state, electron localization

PACS: 33.80.Rv, 31.30.Gs, 33.20.Tp **DOI:** 10.1088/1674-1056/24/4/043302

1. Introduction

The dynamics of a molecule in a strong field has been a popular topic in recent years.[1] Many interesting phenomena, such as above-threshold dissociation and below-threshold dissociation,[2–4] bond hardening and bond softening,[5,6] high-order harmonic generation (HHG),[7–9] and Coulomb explosion[10,11] have been investigated. The HHG is the most attractive effect to be used to generate isolated attosecond pulses.[12] Its physical process can be well understood through the semiclassical three-step model:[13] tunneling, acceleration, and recombination. Due to its additional degrees of freedom and its more complicated structure, the HHG process of a molecule is different from that of an atom. With two nuclei, the ionized electrons can recombine with either the parent ion or the neighbor ion. In recent years, more attention has been paid to the HHG from a symmetric molecular ion. Yu *et al.*[14] have shown that the electron transfer in the two potential wells of H_2^+ induces an efficient molecular plateau, which can be used to generate an intense isolated pulse. Yuan and Bandrauk[15] have demonstrated that the circularly polarized harmonic spectrum from H_2^+ can be generated in the combination of a circularly polarized laser pulse and a static electric field. Bao *et al.*[16] have investigated the harmonic emission from H_2^+ in a superposition of two lowest states. Guo *et al.*,[17] and Feng and Chu[18] have proven that symmetric molecular HHG is sensitive to the initial vibrational states and that more intense harmonics are generated from the lighter isotopes. Ge *et al.*[19] have found that a short trajectory dominates the molecular HHG in a few-cycle laser field and an isolated 129-as pulse can be obtained.

Based on the numerous investigations about the molecular HHG from symmetric molecules, increasing attention has been paid to asymmetric molecules.[20–22] As the simplest asymmetric molecule, HeH^{2+} has now been widely studied. Bian and Bandrauk[23–25] have proposed that the laser-induced electron transfer plays an important role in harmonic emission from HeH^{2+}. Feng and Chu[26] have further shown that the excited effect is a general character of asymmetric molecules. Chen and Zhang[27] have revealed that the role of excited states of HeH^{2+} can be detected via the harmonic emission times. Lu *et al.*[28] have studied the electron localization of HeH^{2+} to isolate and enhance the molecular plateau by adjusting carrier-envelope phase. Moreover, with a longer mean lifetime of the first excited state for HeH^{2+},[29] electrons can transit from the first excited state to the ground state (i.e., from the nucleus H^+ to the nucleus He^{2+}) in an intense laser field. Hence, the electrons can be ionized from and recombine into either the nucleus H^+ or the nucleus He^{2+}. In other words, multiple recombination channels will contribute to the HHG from HeH^{2+}, and the detailed distinguishing of these channels has been presented in our previous study.[30] Additionally, the ionizations from different nuclei depend on the electron distribution. In this paper, we will research the electron localization in an harmonic emission by comparing the HHG from HeH^{2+}

*Project supported by the National Natural Science Foundation of China (Grant No. 11404204), the Key Project of Chinese Ministry of Education (Grant No. 211025), the Research Fund for the Doctoral Program of Higher Education of China (Grant No. 20111404120004), the Natural Science Foundation for Young Scientists of Shanxi Province, China (Grant No. 2009021005), and the Innovation Project for Postgraduates of Shanxi Province, China (Grant No. 20133081).

†Corresponding author. E-mail: sxxymiao@126.com

© 2015 Chinese Physical Society and IOP Publishing Ltd

with that from HeD^{2+} at different vibrational states. The results show that ionization process at the lowest vibrational state mainly originates from electrons localized around the nucleus H^+ (D^+), and the harmonic intensity of HeH^{2+} is 1.3 orders of magnitude stronger than that of HeD^{2+} in a high-order harmonic region. However, with the increase of the initial vibrational level, the electron transfer from the nucleus D^+ to the nucleus He^{2+} is prominently enhanced. For HeD^{2+}, considerable numbers of electrons localized around the nucleus He^{2+} can be ionized so that the difference in harmonic efficiency decreases at a higher vibrational state. Nevertheless, the difference in harmonic spectral structure increases. Due to the more intense interference of multiple recombination channels, an evident minimum can be observed in the HHG spectrum of HeH^{2+}.

2. Numerical method

The one-dimensional numerical simulation for asymmetric diatomic molecules HeH^{2+} and HeD^{2+} in a strong laser field has been performed by solving the non-Born–Oppenheimer time-dependent Schrödinger equation (TDSE) via parallel computer code LZH-DICP.[30–33] The initial state is prepared in a $2p\sigma$ state. Atomic units (a.u.) are used throughout this paper. The linear laser field is along with the molecular axis, and in the dipole approximation and the length gauge, the TDSE reads

$$\mathrm{i}\frac{\partial\psi(R,z;t)}{\partial t} = [T_\mathrm{n} + T_\mathrm{e} + V_\mathrm{c} + V(t)]\,\psi(R,z;t), \tag{1}$$

$$T_\mathrm{n} = -\frac{1}{2\mu_\mathrm{n}}\frac{\partial^2}{\partial R^2},\quad T_\mathrm{e} = -\frac{1}{2\mu_\mathrm{e}}\frac{\partial^2}{\partial z^2}, \tag{2}$$

$$V_\mathrm{c} = \frac{C_\mathrm{He}C_\mathrm{H(D)}}{\sqrt{R^2+0.01}} - \frac{C_\mathrm{H(D)}}{\sqrt{(z-z_\mathrm{H(D)})^2+0.03}} - \frac{C_\mathrm{He}}{\sqrt{(z-z_\mathrm{He})^2+0.03}}, \tag{3}$$

$$V(t) = \left[\frac{C_\mathrm{He}M_\mathrm{H(D)} - C_\mathrm{H(D)}M_\mathrm{He}}{M_\mathrm{H(D)}+M_\mathrm{He}}R + \left(1+\frac{C_\mathrm{H(D)}+C_\mathrm{He}-1}{M_\mathrm{He}+M_\mathrm{H(D)}+1}\right)z\right]\times E(t), \tag{4}$$

where R and z are internuclear distance and electronic coordinate, respectively; μ_n and μ_e are the reduced mass of nuclei He^{2+} and $H^+(D^+)$, M_He and $M_\mathrm{H(D)}$, respectively; C_He and $C_\mathrm{H(D)}$ are the electric charges of the nuclei He^{2+} and $H^+(D^+$, respectively; z_He and $z_\mathrm{H(D)}$ are the positions of the nuclei He^{2+} and $H^+(D^+)$; V_c and $V(t)$ are the Coulomb potential and the interaction potential of HeH^{2+} with the laser pulse; and, $E(t)$ is the electric field that is a seven-optical-cycle (o.c.) trapezoidal field with two cycles ramp on, three cycles constant and two cycles ramp off. In addition, 1 o.c. = 5.34 fs corresponds to the wavelength (1600 nm) of the laser pulse. To solve the TDSE above mentioned, we use the standard second-order split-operator method.[34–36] To guarantee the calculation convergence, the grid ranges from 0 a.u. to 30 a.u. in the R direction and from –100 a.u. to 100 a.u. in the z direction, with 299 and 999 points, respectively. The time step is set to be 0.1 a.u.

The HHG spectrum ($P_A(\omega)$) is obtained by the Fourier transform of the time-dependent dipole acceleration $a(t)$,

$$P_\mathrm{A}(\omega) = \left|\frac{1}{\sqrt{2\pi}}\int a(t)\,\mathrm{e}^{-\mathrm{i}\omega t}\,\mathrm{d}t\right|^2. \tag{5}$$

The time-frequency distribution is displayed to provide more information about the harmonic emission from an asymmetric molecular ion[37]

$$d_\omega(t) = \int a(t')\sqrt{\omega_0}W\left(\omega_0\left(t'-t\right)\right)\mathrm{d}t', \tag{6}$$

where $W(\omega_0(t'-t))$ is the Morlet wavelet, which is expressed as

$$W(x) = \left(\frac{1}{\sqrt{\tau}}\right)\mathrm{e}^{\mathrm{i}x}\,\mathrm{e}^{-x^2/2\tau^2}. \tag{7}$$

3. Numerical results and discussion

Figure 1(a) shows the harmonic spectra of HeH^{2+} (red solid line) and HeD^{2+} (blue dashed line) at the lowest vibrational state ($v=0$) irradiated by a 1600-nm trapezoidal pulse with a peak intensity of 5×10^{14} W/cm^2, as shown in Fig. 1(b). It can be seen that the HHG spectra share some similar characters: the harmonic intensity rapidly decays for the first few-order harmonics, which is followed by a modulating plateau. However, there is still an obvious difference. In the high-order harmonic region marked by the horizontal arrow, the harmonic efficiency of HeH^{2+} is nearly 1.3 orders of magnitude stronger than that of HeD^{2+}. It is known that the harmonic efficiency is sensitive to the ionization probability. To explain the enhancement phenomena above mentioned, the relevant time-dependent total ionization probabilities of HeH^{2+} (red solid line) and HeD^{2+} (blue dashed line) at $v=0$ presented in Fig. 2(a) are calculated by a flux operator and the "virtual director" method.[38] The relevant time-dependent total ionization probability is expressed as

$$C(t) = \int_0^t \mathrm{d}t' \int_0^{R_\mathrm{s}} \mathrm{d}R j_z(R,z_\mathrm{s};t'), \tag{8}$$

where j_z is the flux operator, $z_\mathrm{s}=25$ a.u. is the position for flux analysis, and $R_\mathrm{s}=25$ a.u. is the absorbing position in the present work. Clearly, the ionization probability of HeH^{2+} (62%) is much higher than that of HeD^{2+} (16%) at the end of laser pulse. However, the former is lower than the latter in a time range from $t=2.5$ o.c. to $t=3.5$ o.c. as shown in Fig. 2(b). To understand the difference in the ionization

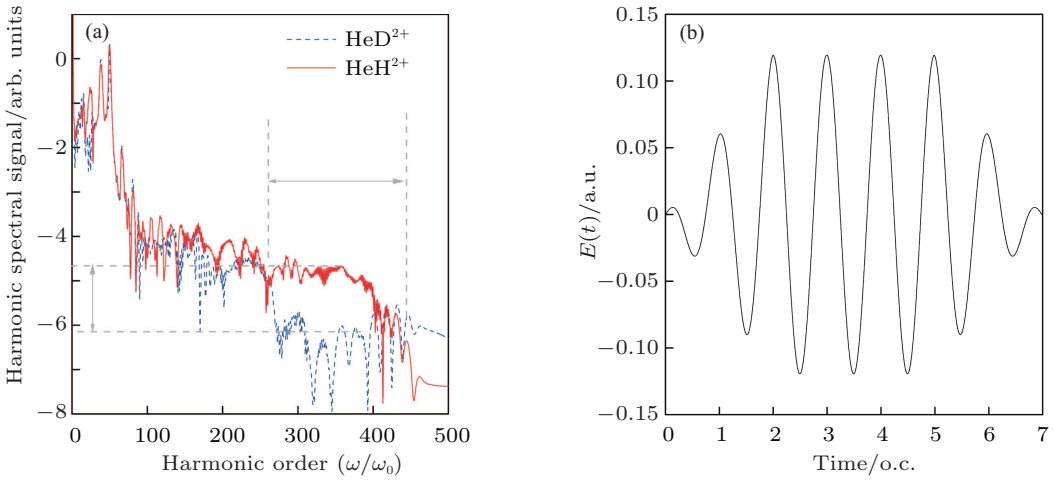


Fig. 1. (color online) (a) High-order harmonic spectra of HeH^{2+} (red solid line) and HeD^{2+} (blue dashed line) at $\nu = 0$. (b) Sketch of the trapezoidal laser pulse with a wavelength of 1600 nm and a peak intensity of 5×10^{14} W/cm^2. The total pulse lasts for seven optical cycles (o.c.).

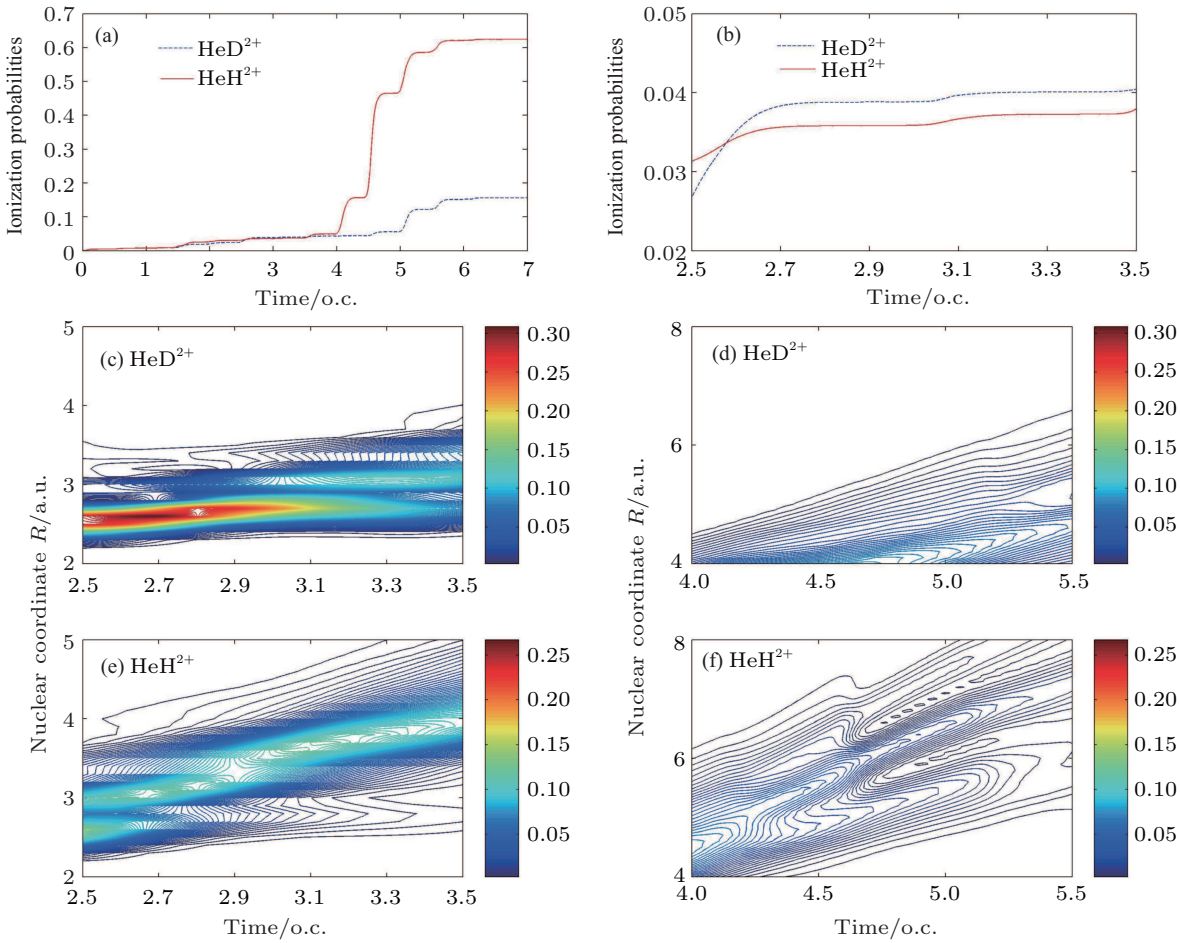


Fig. 2. (color online) With the same laser parameters as those in Fig. 1(a) the ionization probabilities of HeH^{2+} (red solid line) and HeD^{2+} (blue dashed line), (b) the enlargement of the ionization probabilities in a time range from $t = 2.5$ o.c. to $t = 3.5$ o.c. ((c) and (d)) ((e) and (f)) the time evolutions of nuclear probability densities of HeD^{2+} (HeH^{2+}) in time ranges from $t = 2.0$ o.c. to $t = 3.5$ o.c. and from $t = 4.0$ o.c. to $t = 5.5$ o.c., respectively.

process between HeH^{2+} and HeD^{2+}, we investigate the relevant nuclear probability density distributions in different time ranges. As depicted in Figs. 2(c) and 2(e), the wave packets are almost localized in a smaller region (i.e., less than 4 a.u.) from $t = 2.5$ o.c. to $t = 3.5$ o.c. In this case, the electrons are difficult to ionize and nuclear wave packet probability density is a key factor in the ionization process. Since the nuclear probability density distribution of HeD^{2+} in Fig. 2(c) is much stronger than that of HeH^{2+} in Fig. 2(e), more electrons can be ionized from HeD^{2+}. As a result, the ionization probability of the former is higher than that of the latter. However, the nuclear wave packet probability density of HeH^{2+} in Fig. 2(f)

is close to that of HeD^{2+} in Fig. 2(d) in a time range from $t = 4.0$ o.c. to $t = 5.5$ o.c. Moreover, the wave packets of HeH^{2+} can extend to a far larger internuclear distance. Taking these two factors into account, the ionization process of HeH^{2+} will be enhanced predominantly from $t = 4.0$ o.c. to $t = 5.5$ o.c. In short, the difference in harmonic efficiency between two ions at $v = 0$ is probably ascribed to the intense ionization process in a time range from $t = 4.0$ o.c. to $t = 5.5$ o.c. With a longer lifetime of the first excited state for asymmetric molecular ion, the electron localization on different nuclei may play an important role in the harmonic emission process.[23–25] Nevertheless, we cannot estimate the contributions of electrons around either nucleus to harmonic emission directly just according to the nuclear wave packet probability density. More detailed information is still desired.

To obtain a clear insight, we first adopt the double-well model to illustrate the electronic motion around either nucleus. The electronic motions around the nucleus H^+ in Fig. 3(a) and around the nucleus He^{2+} in Fig. 3(b) are taken as an example. The x axis shows the electronic coordinate z, and the y axis shows the combined energy of Coulomb potential V_c and static field potential Fz. The electric field amplitude F corresponds to the peak laser intensity. Additionally, the dash–dotted curve and solid curve represent the combined energy for $F > 0$ and $F < 0$, respectively. The red (blue)-solid arrow represents the ionization process (electron transfer process). The green (red)-dashed arrow represents the homonuclear (heteronuclear) recombination. The magenta dashed arrow represents the intermolecular recombination. As shown in Fig. 3(a), at field $F > 0$, the potential well of the nucleus He^{2+} is dressed down while the potential of the nucleus H^+ is dressed up. So some electrons around the nucleus H^+ can transit to the nucleus He^{2+}, as illustrated by the downward blue-solid arrow directing to A. After half an optical cycle (i.e., $F < 0$), the potential well of the nucleus He^{2+} is dressed up while the potential of the nucleus H^+ is dressed down. These electrons will then directly return back to recombine with the nucleus H^+, as illustrated by the magenta-dashed arrow directing to A_1. Other electrons around the nucleus H^+ may tunnel the barrier and thus become ionized out, as indicated by the red-solid arrow directing to B. After acceleration in the external field, the ionized-out electrons will recombine with either the homonuclear ion (i.e. H^+) or the heteronuclear ion (i.e. He^{2+}), as indicated by the green-dashed arrow directing to B_1 and the red-dashed arrow directing to B_2, respectively. As illustrated in Fig. 3(b), on the one side, the electrons around the nucleus He^{2+} can be pumped to the nucleus H^+ (blue-solid arrow directing to D). When the laser field changes its direction, some electrons may return back to recombine with the nucleus He^{2+} due to the resonance (magenta-dashed arrow directing to $D_{1)}$. On the other side, the electrons around the nucleus He^{2+} can also be ionized (red-solid arrow directing to C), and then accelerate in the laser field. After half an optical cycle, these ionized-out electrons may recombine

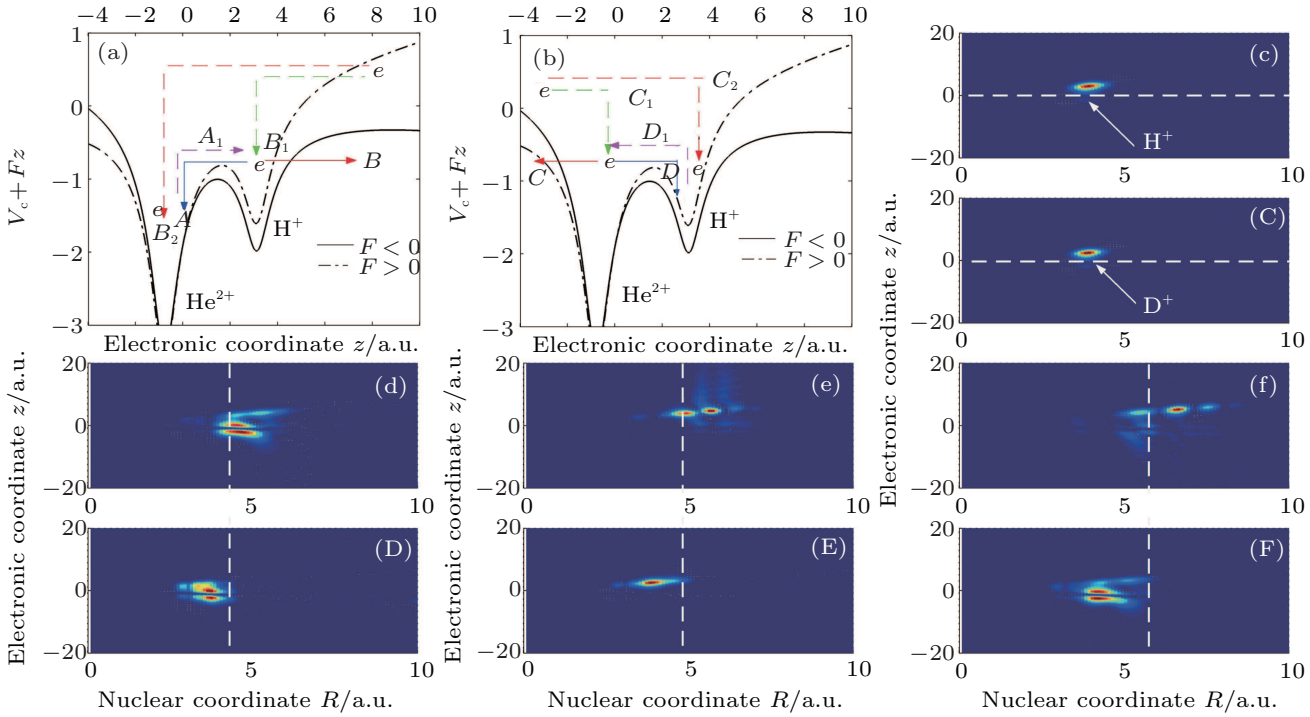


Fig. 3. (color online) (a) and (b) Electron motion around the nucleus H^+ and the nucleus He^{2+}, (c) and (C) the initial electron–nuclear wave packet probability densities of HeH^{2+} and HeD^{2+} (d)–(f) ((D)–(F)) the electron–nuclear probability densities of HeH^{2+} (HeD^{2+}) in a time range from $t = 4.0$ o.c. to $t = 5.0$ o.c. in time steps of $t = 0.5$ o.c.

with either the nucleus He^{2+} (green-dashed arrow directing to C_1) or the nucleus H^+ (red-dashed arrow directing to C_2). In general, when asymmetric molecular ions are exposed to an intense laser field, multiple recombination channels will contribute to the harmonic emission. Furthermore, strong modulations appear in the harmonic spectra as displayed in Fig. 1(a). Next, according to the detailed description of the electronic motion in HeH^{2+}, we will qualitatively estimate the contribution of electrons around either nucleus to harmonic emission. The plots of electron–nuclear probability density distribution $P(R,z) = |\psi(R,z;t)|^2$ of HeH^{2+} and HeD^{2+} at different moments are displayed in Figs. 3(c)–3(f) and in Figs. 3(C)–3(F), respectively. The x axis and y axis represents the nuclear coordinate R and the electronic coordinate z, respectively. Figures 3(c) and 3(C), respectively, illustrate the initial wave packets of HeH^{2+} and HeD^{2+}, which are distributed almost in the region of $z > 0$. For the asymmetric molecular HeH^{2+} (HeD^{2+}), the electrons are localized mainly around the nucleus H^+ (D^+) for $2p\sigma$ state while around the nucleus He^{2+} they are localized for $1s\sigma$ state. So the electrons localized in the region of $z > 0$ and $z < 0$ can be used to show the electronic distribution around the nucleus H^+ (D^+) and He^{2+}, respectively. Considering the obvious difference in ionization probability in a time range from $t = 4.0$ o.c. to $t = 5.0$ o.c., we provide the corresponding electron–nuclear wave packet probability density distributions of HeH^{2+} ((d)–(f)) and HeD^{2+} ((D)–(F)) with a time spacing of 0.5 o.c. The vertical dashed line represents the positions of HeD^{2+} in R direction at different moments. Evidently, considerable numbers of electrons are periodically distributed in the region of $z < 0$ (i.e. the nucleus He^{2+}) around $t = n$ o.c. ($n = 4$ and 5). It is well accordant with the description mentioned above that numbers of electrons can transit from the nucleus H^+ (D^+) to the nucleus He^{2+} at $F > 0$ (i.e. $t = n$ o.c.). With a lighter nuclear mass, the nucleus H^+ moves faster than the nucleus D^+. The larger the internuclear distance is, the more easily the electrons break the constraint of nuclei. Therefore, the ionization probability from the nucleus H^+ is far higher than that from the nucleus D^+. From Fig. 2(a), it can be seen that the difference in ionization probability between HeH^{2+} and HeD^{2+} is rapidly enhanced around 4.5 o.c. Moreover, the electrons are almost distributed around the nucleus H^+ (D^+) for HeH^{2+} (HeD^{2+}) shown in Fig. 3(e) (3(E)). Consequently, the difference in harmonic efficiency between HeH^{2+} and HeD^{2+} at $\nu = 0$ mainly results from the difference in ionization between electrons localized around nucleus H^+ and those around nucleus D^+.

According to the discussion mentioned above, for HeH^{2+} in a $2p\sigma$ state, the electrons around the nucleus He^{2+} mainly originate from the electron transfer from the nucleus H^+. Moreover, electrons around the nucleus H^+ can also directly tunnel the potential barrier and thus become ionized out. This means that the electron transfer process competes with the ionization process for the electrons around the nucleus H^+. It is known that the initial vibrational state greatly affects the ionization process of symmetric molecular ions.[17] For a more complicated structure for an asymmetric molecular ion (HeH^{2+}), the initial vibrational level may also influence the ionization of electrons around the nucleus H^+. It may then indirectly affect the electron transfer process from the nucleus H^+ to the nucleus He^{2+}. Next, we try to investigate the variation of electron localization with the increase of the initial vibrational level. According to Eq. (8), the ionization probabilities of HeH^{2+} and HeD^{2+} in different vibration states (from $\nu = 0$ to $\nu = 5$) are calculated. Figure 4(a) illustrates the corresponding difference in ionization probability ($D_{\rm asy}$) between HeH^{2+} and HeD^{2+}. With the increase of vibrational state, the $D_{\rm asy}$ decreases quickly from 46% for $\nu = 0$ to 0.9% for $\nu = 5$. So the ionization probability of HeD^{2+} is almost identical with that of HeH^{2+} at $\nu = 5$. According to the discussion about the ionization difference at $\nu = 0$, we know that the ionizations of the electrons around nucleus H^+ (D^+) play an important role in the ionization process. How do the electron localization and the corresponding ionization change with the increase of the initial vibrational level in harmonic emission? To obtain more information, figure 4(b) provides the time-dependent total ionization probabilities of HeH^{2+} (red-solid line) and HeD^{2+} (blue-dashed line) at $\nu = 5$. It can be observed that the ionization probability of HeD^{2+} from $t = 4.0$ o.c. to $t = 5.0$ o.c. increases more quickly than that of HeH^{2+}, and then the relevant difference in ionization probability decreases at the end of the laser pulse. The corresponding electron–nuclear wave packet probability density distributions of HeD^{2+} ((c)–(e)) and HeH^{2+} ((f)–(h)) at $\nu = 5$ are demonstrated. Obviously, the nucleus H^+ extends to a larger internuclear distance faster than the nucleus D^+ in R direction. Moreover, the corresponding ionization potential is suppressed with the increase of the vibrational state.[17] So considerable numbers of electrons around the nucleus H^+ will be ionized quickly, and then the transferred electrons to the nucleus He^{2+} tend to be fewer. Compared with the electrons around HeH^{2+}, the electrons around the nucleus D^+ are relatively difficult to be ionized out, and thus more electrons are then transferred from the nucleus D^+ to the nucleus He^{2+}. As observed from Figs. 4(c) to 4(h), the probability density around the nucleus He^{2+} for HeD^{2+} is larger than that for HeH^{2+} in a time range from $t = 4.0$ o.c. to $t = 5.0$ o.c. In other words, with the increase of the initial vibrational level, more electrons tend to localize around the nucleus He^{2+}. Additionally, the relevant constraint of nucleus He^{2+} to electrons tends to be weaker, and then the ionization from the nucleus He^{2+} will be enhanced prominently. Therefore, it is the dramatic enhancement of ionization from the nucleus He^{2+} for HeD^{2+}at

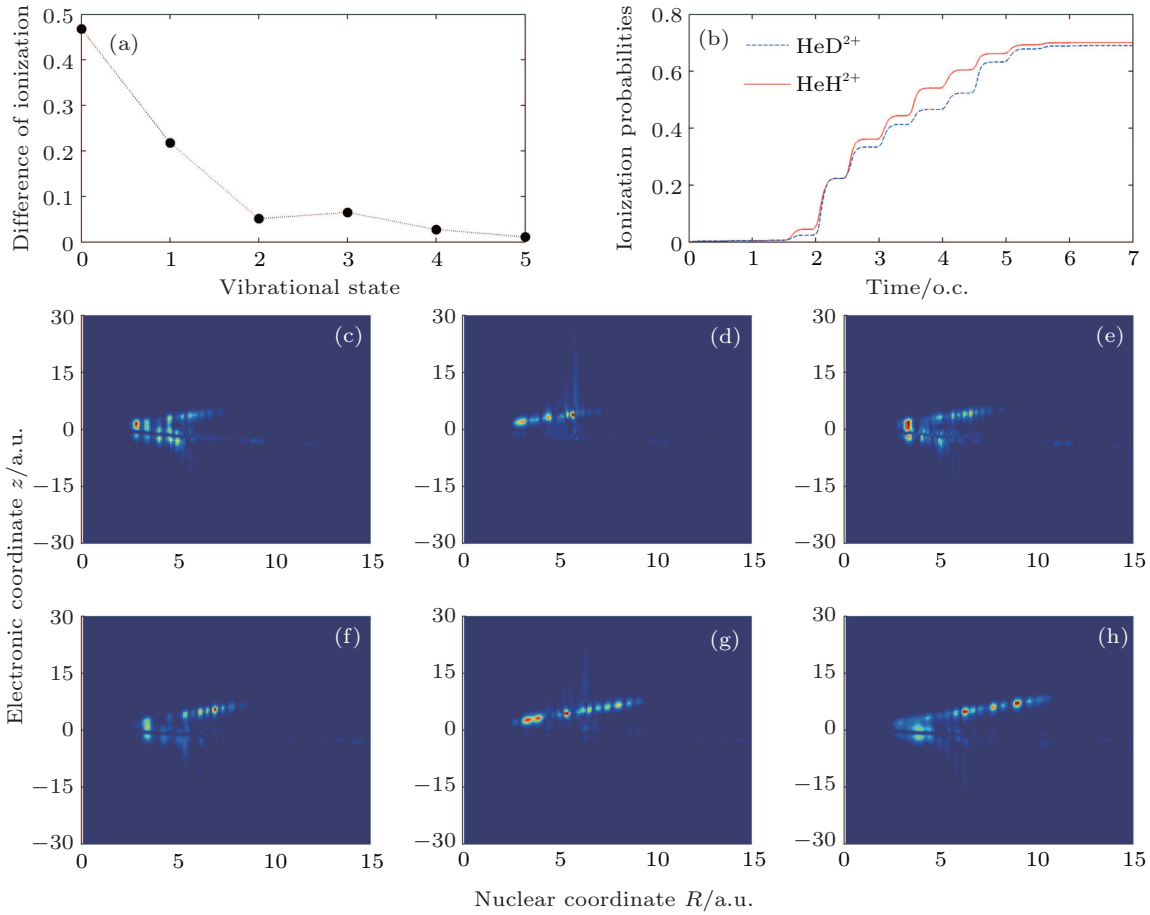


Fig. 4. (color online) (a) Difference in ionization probability between HeH^{2+} and HeD^{2+} versus initial vibrational state from $v = 0$ to $v = 5$, (b) ionization probabilities of HeH^{2+} (red-solid line) and HeD^{2+} (blue-dashed line) for $v = 5$, (c)–(e) and (f)–(h) the electron–nuclear probability densities of HeD^{2+} and HeH^{2+} in time range from $t = 4.0$ o.c. to $t = 5.0$ o.c. in time steps of $t = 0.5$ o.c., respectively.

$v = 5$ that leads to almost the same ionization probability as that for HeH^{2+}. In the following simulation, we will focus on the relevant variations of the harmonic spectra of HeH^{2+} and HeD^{2+}.

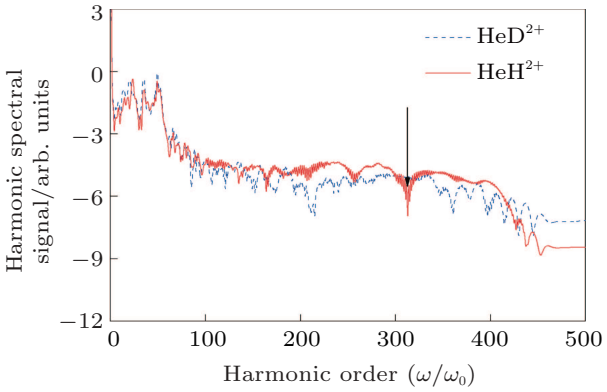


Fig. 5. (color online) High-order harmonic spectra of HeH^{2+} (red-solid line) and HeD^{2+} (blue-dashed line) at $v = 5$.

Figure 5 shows the harmonic spectra of HeH^{2+} (red-solid line) and HeD^{2+} (blue-dashed line) at $v = 5$. With almost identical ionization probabilities, the harmonic efficiencies are nearly the same as each other. Nevertheless, their spectral structures exhibit different characteristics. For instance, there is an additional remarkable minimum indicated by an arrow around the 315th order in harmonic spectrum of HeH^{2+}, although it is not notable in the spectrum of HeD^{2+}. Due to the periodical harmonic emission, the time-frequency distributions of HeH^{2+} and HeD^{2+} in one optical cycle (from $t = 2.3$ o.c. to $t = 3.3$ o.c.) are selected to study the relevant physical mechanisms. Figures 6(a) and 6(c) (Figs. 6(b) and 6(d)) are time-frequency maps of HeH^{2+} (HeD^{2+}) at $v = 0$ and $v = 5$, respectively. It is obvious that multiple recombination channels contribute to the harmonic emission from asymmetric molecular ions in an intense laser field, and the detailed distinguishing of these recombination channels has been discussed in Ref. [30]. With the increase of vibrational level, the higher ionization probability of HeH^{2+} may induce stronger intensities of the recombination channels originating from both the nucleus H^+ and the nucleus He^{2+}. What is more, the long trajectory of the recombination channel originating from the nucleus H^+ (LRH) and the interference of multiple recombination channels (IM1) are both enhanced greatly. And then the minimum in the spectrum of HeH^{2+} may be attributed to two factors. One is the interference between the long trajec-

tory and the short one originating from the nucleus H^+ (IMT), and the other is the interference of the recombination channels originating from the nucleus H^+ and the nucleus He^{2+} (i.e. IM1). To investigate the original mechanism, we compare the time-frequency map of HeD^{2+} at $v = 0$ with that at $v = 5$. It is found that both the long trajectory of the recombination channel originating from the nucleus D^+ (LRD) and the interference of multiple recombination channels of HeD^{2+} (IM2) are also enhanced with the increase of vibrational state. However, there is no noticeable suppression in the harmonic spectrum of HeD^{2+} around 315th order at $v = 5$. Next, the enlargements of the time-frequency distributions of HeH^{2+} and HeD^{2+} from 250th order to 350th order are shown in the insets of Figs. 6(c) and 6(d), respectively. It is worth noting that around the 315th order, the intensity of the LRH is nearly the same as that of the LRD while the intensity of the IM1 is much more intense than that of the IM2. As a result, it may be the stronger IM1 rather than the IMT that induces the evident suppression in the harmonic spectrum of HeH^{2+} at $v = 5$.

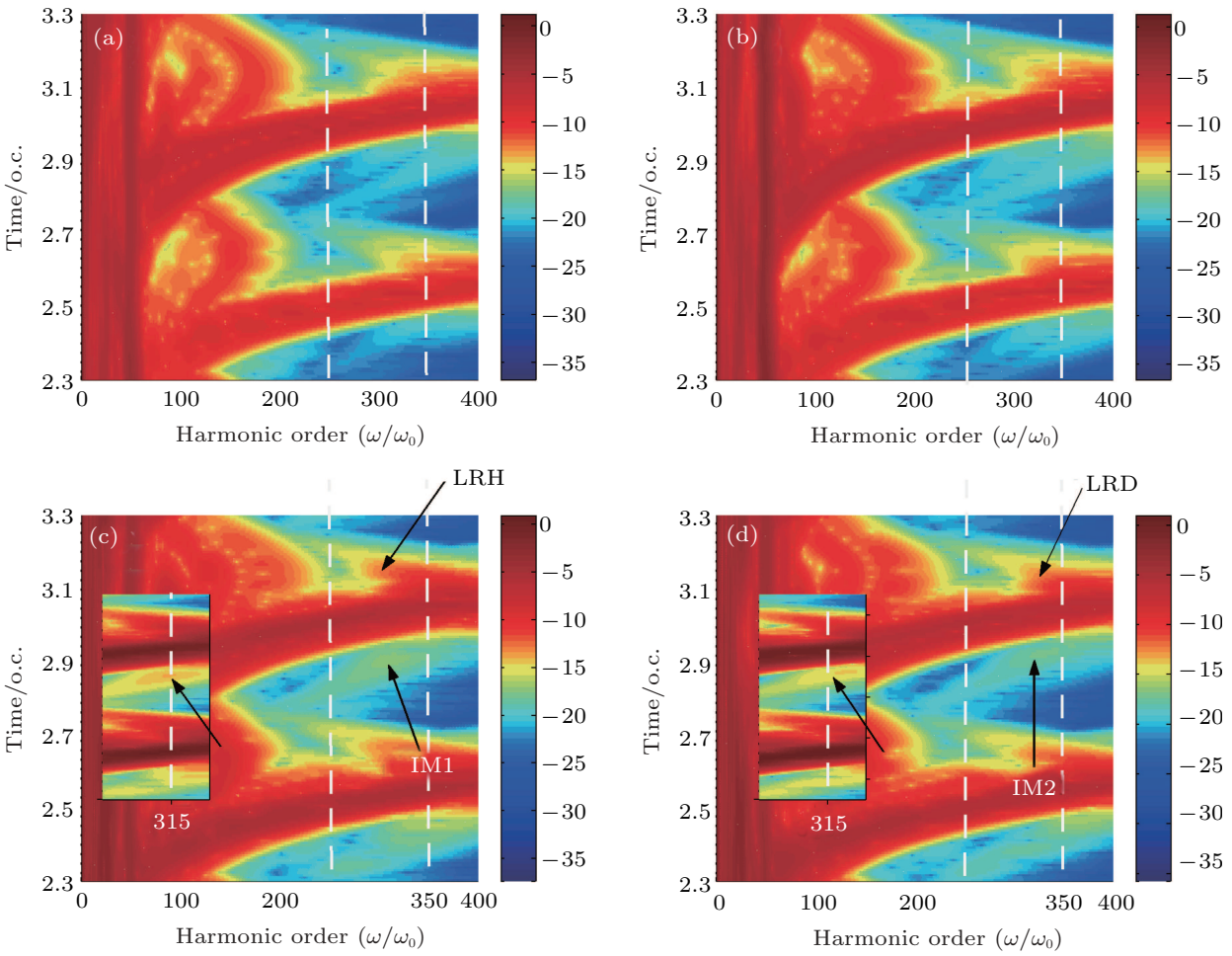


Fig. 6. (color online) (a) and (b) ((c) and (d)) time-frequency distributions for HeH^{2+} and HeD^{2+} at $v = 0$ (at $v = 5$) in a time range from $t = 2.3$ o.c. to $t = 3.3$ o.c., respectively. The insert shows the enlargement of time-frequency distributions from 250th order to 350th order.

4. Conclusions

In this paper, the electron localization in the harmonic emission is investigated by numerically solving the non-Born–Oppenheimer time-dependent Schrödinger equation. According to the comparison of harmonic emission of HeH^{2+} with that of HeD^{2+} at different vibrational states, we qualitatively estimate the contributions of electrons around two nuclei to the ionization process. At the lowest vibrational state, the ionizations of electrons localized around the nucleus H^+ (D^+) mainly dominate the ionization process in harmonic emission, which leads to an harmonic intensity of HeH^{2+} that is 1.3 orders of magnitude stronger than that of HeD^{2+} in a high-order harmonic region. With the increase of the initial vibrational level, the electron transfer from the nucleus D^+ to the nucleus He^{2+} is enhanced and more electrons tend to be localized around the nucleus He^{2+}. In this case, the ionizations of electrons around the nucleus He^{2+} are enhanced prominently, and then the harmonic efficiency of HeD^{2+} is almost the same as that of HeH^{2+}. However, the spectral structures are different. The stronger interference of multiple recombination channels may lead to an obvious minimum in the HHG spectrum of HeH^{2+}.

Acknowledgement

The authors sincerely thank Prof. Han Ke-Li and Dr. Lu Rui-Feng for providing us with the LZH-DICP code.

References

[1] Chang Z H and Corkum P 2010 *J. Opt. Soc. Am. B* **27** B9
[2] Hua J J and Esry B D 2009 *J. Phys. B: At. Mol. Opt. Phys.* **42** 085601
[3] Roudnev V, Esry B D and Ben-Itzhak I 2004 *Phys. Rev. Lett.* **93** 163601
[4] Posthumus J H, Plumridge J, Frasinski L J, Coding K, Dival E J, Langley A J and Taday P F 2000 *J. Phys. B: At. Mol. Opt. Phys.* **33** L563
[5] Frasinski L J, Posthumus J H, Plumridge J, Coding K, Dival E J and Langley A J 1999 *Phys. Rev. Lett.* **83** 3625
[6] Wang P Q, Sayler A M, Carnes K D, Xia J F, Smith M A, Esry B D and Ben-Itzhak I 2005 *J. Phys. B: At. Mol. Opt. Phys.* **38** L251
[7] Huang P, Xie X T, Lü X Y, Li J H and Yang X X 2009 *Phys. Rev. A* **79** 043806
[8] Du H N and Miao X Y 2012 *Spectrosc. Lett.* **45** 609
[9] Han Y C and Madsen L B 2013 *Phys. Rev. A* **87** 043404
[10] Shi H T and Miao X Y 2013 *Chin. Phys. Lett.* **30** 063101
[11] Zhang C P and Miao X Y 2013 *Chin. Phys. Lett.* **30** 103101
[12] Zheng Y H, Zeng Z N, Li R X and Xu Z Z 2012 *Phys. Rev. A***85** 023410
[13] Corkum P B 1993 *Phys. Rev. Lett.* **71** 1994
[14] Yu C, He H X, Wang Y H, Shi Q, Zhang Y D and Lu R F 2014 *J. Phys. B: At. Mol. Opt. Phys.* **47** 055601
[15] Yuan K J and Bandrauk A D 2011 *Phys. Rev. A* **83** 063422
[16] Bao J, Chen W B, Zhao Z X and Yuan J M 2011 *J. Phys. B: At. Mol. Opt. Phys.* **44** 195601
[17] Guo Y H, He H X, Liu J Y and He G Z 2010 *J. Mol. Struct: THEOCHEM* **947** 119
[18] Feng L Q and Chu T S 2012 *J. Chem. Phys.* **136** 054102
[19] Ge X L, Wang T, Guo J and Liu X S 2014 *Phys. Rev. A* **89** 023424
[20] Zhang B, Chen Y J, Jiang X Q and Sun X D 2013 *Phys. Rev. A* **88** 053428
[21] Etches A, Gaarde M B and Madsen L B 2012 *Phys. Rev. A* **86** 023818
[22] Chen Y J, Fu L B and Liu J 2013 *Phys. Rev. Lett.* **111** 073902
[23] Bian X B and Bandrauk A D 2011 *Phys. Rev. A* **83** 023414
[24] Bian X B and Bandrauk A D 2011 *Phys. Rev. A* **83** 041403
[25] Bian X B and Bandrauk A D 2012 *Phys. Rev. A* **86** 053417
[26] Feng L Q and Chu T S 2013 *Commun. Comput. Chem.* **1** 52
[27] Chen Y J and Zhang B 2012 *Phys. Rev. A* **86** 023415
[28] Lu R F, Chao Y, Wang Y H, Shi Q and Zhang Y D 2014 *Phys. Lett. A* **378** 90
[29] Ben-Itzhak I, Gertner I, Heber O and Rosner B 1993 *Phys. Rev. Lett.* **71** 1347
[30] Miao X Y and Zhang C P 2014 *Phys. Rev. A* **89** 033410
[31] Lu R F, Zhang P Y and Han K L 2008 *Phys. Rev. E* **77** 066701
[32] Miao X Y and Zhang C P 2014 *Laser Phys. Lett.* **11** 115301
[33] He H X, Lu R F, Zhang P Y, Guo Y H, Han K L and He G Z 2011 *Phys. Rev. A* **84** 033418
[34] Chu T S, Zhang Y and Han K L 2006 *Int. Rev. Phys. Chem.* **25** 201
[35] Hu J, Han K L and He G Z 2005 *Phys. Rev. Lett.* **95** 123001
[36] Miao X Y and Du H N 2013 *Phys. Rev. A* **87** 053403
[37] Tong X M and Chu Sh I 2000 *Phys. Rev. A* **61** 021802
[38] Feuerstein B and Thumm U 2003 *Phys. Rev. A* **67** 043405